Inorg. Chem. **2008**, *47*, 10998−11009

Metalloradical Complexes of Manganese and Chromium Featuring an Oxidatively Rearranged Ligand

Remle Çelenligil-Çetin,[‡] Patrina Paraskevopoulou,[†] Nikolia Lalioti,[¶] Yiannis Sanakis,[⊥] Richard J. Staples,[§] Nigam P. Rath,[#] and Pericles Stavropoulos*[,†]

Department of Chemistry, Missouri University of Science and Technology, Rolla, Missouri 65409, Department of Chemistry, Boston University, Boston, Massachusetts 02215, Department of Chemistry and Chemical Biology, Harvard University, Cambridge, Massachusetts 02138, Department of Chemistry, University of Patras, Patras 26500, Greece, Department of Chemistry and Biochemistry, University of Missouri-St. Louis, St. Louis, Missouri 63121, and the Institute of Materials Science, NCSR "Demokritos", Ag. Paraskevi 15310, Greece

Received July 2, 2008

Redox events involving both metal and ligand sites are receiving increased attention since a number of biological processes direct redox equivalents toward functional residues. Metalloradical synthetic analogues remain scarce and require better definition of their mode of formation and subsequent operation. The trisamido-amine ligand $[(RNC_6H_4)_3N]^{3-}$, where R is the electron-rich 4-*t*-BuPh, is employed in this study to generate redox active residues in manganese and chromium complexes. Solutions of $[(L^1)Mn(II)\text{-}THF]^-$ in THF are oxidized by dioxygen to afford $[(L^1{}_{re-1})Mn(III)\text{-}(O)_2\text{-}Mn(III)(L^1{}_{re-1})]^{2-}$ as the major product. The rare dinuclear manganese (III,III) core is stabilized by a rearranged ligand that has undergone an one-electron oxidative transformation, followed by retention of the oxidation equivalent as a π radical in an *o*-diiminobenzosemiquinonate moiety. Magnetic studies indicate that the ligand-centered radical is stabilized by means of extended antiferromagnetic coupling between the $S = 1/2$ radical and the adjacent $S = 2$ Mn(III) site, as well as between the two Mn(III) centers via the dioxo bridge. Electrochemical and EPR data suggest that this system can store higher levels of oxidation potency. Entry to the corresponding Cr(III) chemistry is achieved by employing $CrCl_3$ to access both $[(L^1)Cr(III)\text{-}THF]$ and $[(L^1{}_{re-1})Cr(III)\text{-}THF(Cl)]$, featuring the intact and the oxidatively rearranged ligands, respectively. The latter is generated by ligand-centered oxidation of the former compound. The rearranged ligand is perceived to be the product of an one-electron oxidation of the intact ligand to afford a metal-bound aminyl radical that subsequently mediates a radical 1,4-(*N*-to-*N*) aryl migration.

Introduction

Many manganese[1] and chromium[2] reagents are well established as oxidizing entities, owing to the oxophilicity of these metals and their rich redox capabilities. These attributes also contribute, either beneficially or detrimentally, to multiple engagements of both metals in critical biological functions.[3,4] Much more is known about manganese,[3] whose involvement, among others, in catalases, superoxide dismutases, the oxygen-evolving complex of photosystem II, and most recently, in ribonucleotide reductase (class IV RNR),[5] has been the center of significant attention. In this context, the $Mn(\mu\text{-}O)_2Mn$ core is a well-recognized feature of manganese chemistry, encompassing the more rare $Mn(III)(\mu\text{-}O)_2Mn(III)$ oxidation level and the more common, mixed-valent $Mn(III)(\mu\text{-}O)_2Mn(IV)$ and high-valent $Mn(IV)(\mu\text{-}O)_2Mn(IV)$ counterparts.[3b,6] While most of the discussion is currently centered on metal-residing oxidation equivalents, the involvement of tyrosyl radicals in the oxygen-evolving PSII center,[7] and the recent discovery of a cysteinyl radical associated with a dioxygen-generated, Mn(IV)-Fe(III)-

* To whom correspondence should be addressed.
‡ Boston University.
† Missouri University of Science and Technology.
¶ University of Patras.
⊥ NCSR "Demokritos".
§ Harvard University.
# University of Missouri-St. Louis.

(1) (a) Larrow, J. F.; Jacobsen, E. N. *Topics Organomet. Chem.* **2004**, *6*, 123–152. (b) Lee, T. V. In *Comprehensive Organic Synthesis*; Trost, B. M., Fleming, I., Eds.; Pergamon: Oxford, 1990; Vol. *7*, pp 291−303.
(2) (a) Luzzio, F. A. *Org. React.* **1998**, *53*, 1–221. (b) Ley, S. V.; Maddin, A. In *Comprehensive Organic Synthesis*; Trost, B. M., Fleming, I., Eds.; Pergamon, Oxford, 1990; Vol *7*, pp 251−289.

10.1021/ic801219u CCC: $40.75
Published on Web 10/21/2008

containing cofactor in the RNR of the bacterium *Chlamydia trachomatis*, is expected to fuel interest in the generation and function of redox-active residues in tandem with Mn centers.[5]

We have previously shown[8] that compound $[(L^1)Fe(II)\text{-}THF]^-$, where L^1 is the trisamido-amine ligand $[(4\text{-}t\text{-}Bu\text{-}C_6H_4)NC_6H_4]_3N^{3-}$ (Chart 1), can be oxidized by dioxygen in THF to afford $[(L^1_{re-1})Fe\text{-}O\text{-}Fe(L^1_{re-1})]$ as a minor product. The ligand in this diferric μ-oxo species has undergone one-electron oxidative rearrangement, while the oxidation equivalent is retained as a π radical. In the present study we demonstrate that the corresponding Mn(II) complex can generate a rare Mn(III)$(\mu\text{-}O)_2$Mn(III) core-containing analogue, as the major product of its reaction with dioxygen. Moreover, the $[(L^1_{re-1})Mn(III)]$ oxidation level can be replicated in a mononuclear $[(L^1_{re-1})Cr(III)]$-containing compound, using $CrCl_3$ as oxidant.

Experimental Section

General Considerations. All operations were performed under anaerobic conditions under a pure dinitrogen or argon atmosphere using Schlenk techniques on an inert gas/vacuum manifold or in a drybox (O_2, H_2O < 1 ppm). Anhydrous diethyl ether, methylene chloride, acetonitrile, tetrahydrofuran, hexane, pentane, and toluene were purchased from Sigma-Aldrich. Acetone was distilled over drierite. Solvents were degassed by three freeze−pump−thaw cycles. Unless otherwise noted, all other reagents were purchased at the highest purity available. Potassium hydride was provided as dispersion in mineral oil and was thoroughly washed prior to use with copious amounts of tetrahydrofuran followed by hexane. The synthesis of the ligand L^1H_3 has been previously described.[9] ^{1}H NMR and ^{13}C NMR spectra were recorded on Varian XL-400, Varian INOVA/UNITY 400 MHz, Varian 300 Unity Plus, and Varian 600 MHz FT-HR-NMR spectrometers. FT-IR spectra were obtained on Nicolet Nexus 470, 670, and Magna 750 FT-IR ESP spectrometers and on a Bruker EQUINOX 55 spectrometer with a single reflection accessory (DuraSamplIR II by SensIR Technologies) equipped with a diamond element. UV−vis spectra were obtained on a Hewlett-Packard 8452A diode array spectrometer and a Varian Cary 50 spectrophotometer. EI and CI mass spectra were obtained on a Finnigan MAT-90 mass spectrometer. HRMS (ESI) data were collected on an Applied Biosystems QStar Pulsar instrument with a microspray ion source, located at the University of Missouri-Columbia. Microanalyses were done by Quantitative Technologies Inc., Whitehouse, NJ, Galbraith Laboratories, Inc., Knoxville, TN, and on an in-house Perkin-Elmer 2400 CHN analyzer.

Dual mode X-band EPR spectra were recorded at the Institute of Materials Science, NCSR "Demokritos", on an extensively upgraded former Bruker ER-200D spectrometer interfaced with a personal computer running appropriate software in the LabView programming environment. The spectrometer was equipped with an Oxford ESR 900 cryostat, an Anritsu MF76A frequency counter, and a Bruker 035 M NMR gaussmeter. The perpendicular mode spectra were obtained with the 4102ST cavity, whereas the parallel mode spectra were obtained with the dual mode cavity, 4116 DM. Simulations of the spectra were performed with the software SpinCount kindly provided to us by Prof. M. P. Hendrich, Department of Chemistry, Carnegie Mellon University, Pittsburgh, PA, USA. X-band EPR spectra were recorded on a Bruker Instruments Model ESP 300 with an EMX upgrade, supported by an APD Cryogenics Co. Cryostat HELI-TRAN model LTR-3, located at the Chemistry Department of Dartmouth College, NH.

Chart 1

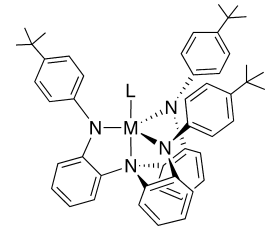

$[(L^1)Mn(II)\text{-}THF][K(THF)_x]$ (1a) and $[(L^1)Mn(II)\text{-}THF]\text{-}(Ph_4P)\cdot 3THF$ (1b). Ligand L^1H_3 (0.343 g, 0.5 mmol) was dissolved in degassed THF (15.0 mL), to which KH (0.060 g, 1.5 mmol) was added. The mixture was stirred overnight until all KH was dissolved. $MnCl_2$ (0.0625 g, 0.5 mmol) was then added as solid to the resulting yellow THF solution. This mixture was stirred for another 10 h to give a pale yellow solution. This solution was

(3) (a) Dismukes, G. C. *Chem. Rev.* **1996**, *96*, 2909–2926. (b) Mukhopadhyay, S.; Mandal, S. K.; Bhaduri, S.; Armstrong, W. H. *Chem. Rev.* **2004**, *104*, 3981–4026. (c) Wu, A. J.; Penner-Hahn, J. E.; Pecoraro, V. L. *Chem. Rev.* **2004**, *104*, 903–938. (d) Jedrzejas, M. J.; Setlow, P. *Chem. Rev.* **2001**, *101*, 607–618. (e) Gold, M. H.; Youngs, H. L.; Sollewijn, G.; Maarten, D. In *Metal Ions in Biological Systems: Manganese and Its Role in Biological Processes*; Sigel, A., Sigel, H., Eds.; Marcel Dekker, Inc.: New York, Basel, 2000; Vol. *37*, pp 559−586. (f) Ash, D. E.; Cox, J. D.; Christianson, D. W. In *Metal Ions in Biological Systems: Manganese and Its Role in Biological Processes*; Sigel, A., Sigel, H., Eds.; Marcel Dekker, Inc.: New York, Basel, 2000; Vol. *37*, pp 407−428. (g) Bogumil, R.; Kappl, R.; Huttermann, J. In *Metal Ions in Biological Systems: Manganese and Its Role in Biological Processes*; Sigel, A., Sigel, H., Eds.; Marcel Dekker, Inc.: New York, Basel, 2000; Vol. *37*, pp. 365−405. (h) Rusnak, F. In *Metal Ions in Biological Systems: Manganese and Its Role in Biological Processes*; Sigel, A., Sigel, H., Eds.; Marcel Dekker, Inc.: New York, Basel, 2000; Vol. *37*, pp 305−343. (i) Crowley, J. D.; Traynor, D. A.; Weatherburn, D. C. In *Metal Ions in Biological Systems: Manganese and Its Role in Biological Processes*; Sigel, A., Sigel, H., Eds.; Marcel Dekker, Inc.: New York, Basel, 2000; Vol. *37*, pp 209−278. (j) Christianson, D. W.; Cox, J. D. *Annu. Rev. Biochem.* **1999**, *68*, 33–57. (k) Weatherburn, D. C. In *Perspectives on Bioinorganic Chemistry***1996**, *3*, 1−113.

(4) (a) Brautigan, D. L.; Kruszewski, A.; Wang, H. *Biochem. Biophys. Res. Commun.* **2006**, *347*, 769–773. (b) Wang, H.; Kruszewski, A.; Brautigan, D. L. *Biochemistry* **2005**, *44*, 8167–8175. (c) Kawanishi, S.; Inoue, S.; Sano, S. *J. Biol. Chem.* **1986**, *261*, 5952–5958. (d) Shi, X.; Dalal, N. S. *Biochem. Biophys. Res. Commun.* **1988**, *156*, 137–142.

(5) Jiang, W.; Yun, D.; Saleh, L.; Barr, E. W.; Xing, G.; Hoffart, L. M.; Maslak, M.-A.; Krebs, C.; Bollinger, J. M., Jr. *Science* **2007**, *316*, 1188–1191.

(6) (a) Goodson, P. A.; Glerup, J.; Hodgson, D. J.; Michelsen, K.; Pedersen, E. *Inorg. Chem.* **1990**, *29*, 503–508. (b) Goodson, P. A.; Glerup, J.; Hodgson, D. J.; Michelsen, K.; Weihe, H. *Inorg. Chem.* **1991**, *30*, 4909–4914. (c) Manchanda, R.; Brudvig, G. W.; de Gala, S.; Crabtree, R. H. *Inorg. Chem.* **1994**, *33*, 5157–5160. (d) Jensen, A. F.; Su, Z.; Hansen, N. K.; Larsen, F. K. *Inorg. Chem.* **1995**, *34*, 4244–4252. (e) Horner, O.; Charlot, M.-F.; Boussac, A.; Anxolabéhére-Mallart, E.; Tchertanov, L.; Guilhem, J.; Girerd, J.-J. *Eur. J. Inorg. Chem.* **1998**, 721–727. (f) Hureau, C.; Blondin, G.; Cesario, M.; Un, S. *J. Am. Chem. Soc.* **2003**, *125*, 11637–11645. (g) Chen, H.; Tagore, R.; Das, S.; Incarvito, C.; Faller, J. W.; Crabtree, R. H; Brudvig, G. W. *Inorg. Chem.* **2005**, *44*, 7661–7670.

(7) (a) Hoganson, C. W.; Babcock, G. T. *Science* **1992**, *277*, 1953–1956. (b) Petrouleas, V.; Koulougliotis, D.; Ioannidis, N. *Biochemistry* **2005**, *44*, 6723–6728.

(8) Çelenligil-Çetin, R.; Paraskevopoulou, P.; Dinda, R.; Lalioti, N.; Sanakis, Y.; Rawashdeh, A. M.; Staples, R. J.; Sinn, E.; Stavropoulos, P. *Eur. J. Inorg. Chem.* **2008**, 673–677.

(9) (a) Çelenligil-Çetin, R.; Paraskevopoulou, P.; Dinda, R.; Staples, R. J.; Sinn, E.; Rath, N. P.; Stavropoulos, P. *Inorg. Chem.* **2008**, *47*, 1165–1172. (b) Jones, M. B.; MacBeth, C. E. *Inorg. Chem.* **2007**, *46*, 8117–8119.

refrigerated overnight to allow settling of KCl, and was carefully filtered. The filtrate was reduced to 2.0 mL and pentane was allowed to slowly diffuse into this solution at −20 °C to give microcrystalline **1a** at an estimated yield of 60%. The solid was extracted with THF (3.0 mL), and excess $(Ph_4P)Cl$ was added as a solid to this solution until some precipitate was formed. This was filtered and the filtrate was mixed with just enough hexane to initiate precipitation. The precipitate was filtered and the filtrate was allowed to stand at room temperature for a few days to afford X-ray quality orange crystals of **1b** (0.150 g, 25%). UV−vis (THF): λ_{max} (ε (M^{-1} cm^{-1})) 470 (1450), 520 (820). Elemental Analysis: Calcd. for $C_{76}H_{79}MnN_4OP$ (**1**-3THF): C, 79.35; H, 6.92; N, 4.87. Found: C, 79.34; H, 6.34; N, 4.84.

$[(L^1_{re-1})Mn(III)\text{-}(O)_2\text{-}Mn(III)(L^1_{re-1})][K(OEt_2)]_2\cdot C_6H_{14}$ (2). Ligand L^1H_3 (0.343 g, 0.5 mmol) was dissolved in degassed THF (15.0 mL), to which KH (0.060 g, 1.5 mmol) was added. The mixture was stirred overnight until all KH was dissolved. $MnCl_2$ (0.0625 g, 0.5 mmol) was added to this yellow solution as solid and the mixture was allowed to stir for another 10 h to give a pale yellow solution. Dioxygen ("extra dry", 99.999%) was then bubbled through this solution for 2.0 min to generate a dark green-brown solution. This solution was evaporated to dryness under vacuum, extracted with hexane, and filtered. The extract was evaporated to dryness and redissolved in a minimum amount of diethyl ether. The resulting solution was layered with hexane and allowed to stand at room temperature to afford dark green crystals of **2** (0.200 g, 24%). IR (KBr, cm^{-1}): 1591, 1570, 1549, 1527, 1513, 1499, 1481, 1466, 1448, 1409, 1391, 1361, 1315, 1267, 1191, 1158, 1106, 1043, 1017, 924, 866, 830, 739, 707, 675, 636, 612, 589, 583, 555, 493, 479, 467, 450, 435, 412, 404. UV−vis (THF): λ_{max} (ε (M^{-1} cm^{-1})) 276 (4550), 390 (sh), 496 (1810), 720 (sh). Elemental Analysis: Calcd. for $C_{110}H_{136}K_2Mn_2N_8O_4$: C, 72.50; H, 7.52; N, 6.15. Found: C, 71.78; H, 7.83; N, 6.27.

1,3,5′-Tris(4-tert-butylphenyl)-1,3-dihydro-5′H-spiro[benzo[d]imidazole-2,1′-phenazine]·Et_2O (3). Ligand L^1H_3 (0.343 g, 0.5 mmol) was dissolved in degassed THF (15.0 mL), to which KH (0.060 g, 1.5 mmol) was added. The mixture was stirred overnight until all KH was dissolved. $MnCl_2$ (0.0625 g, 0.5 mmol) was added to this yellow solution as solid and the mixture was stirred for another 10 h to give a pale yellow solution. Dioxygen was bubbled through the solution for approximately 15 min until a purple color solution was generated. This solution was evaporated to dryness under vacuum, extracted with diethyl ether and filtered. The filtrate was reduced to a minimum amount and allowed to stand at room temperature to give dark purple crystals of **3** (0.035 g, 10%). ^1H NMR(THF-d_8, 1.73 ppm): δ 7.604 (d, 2H, J = 8.4 Hz), 7.237 (dd, 10H, J = 40.8 Hz, J' = 8.4 Hz), 6.928 (d, 3H, J = 8.4 Hz), 6.779 (t, 1H, J = 7.2 Hz), 6.526 (d, 4H, J = 3.0 Hz), 6.074 (d, 1H, J = 8.4 Hz), 5.978 (dd, 1H, J = 9.6 Hz, J' = 6.6 Hz), 5.667 (d, 1H, J = 9.6 Hz), 1.367 (s, 27H, *tert*-butyl). UV−vis (THF): λ_{max} (ε (M^{-1} cm^{-1})) 296 (3830), 336 (2800), 522 (600). HRMS (ESI): Calcd. for $C_{48}H_{51}N_4$ ($[M + H]^+$): 683.4108. Found: 683.4241.

$[(L^1_{re-1})(Cl)Cr(III)\text{-}THF]\cdot 0.75C_6H_{14}$ (4). Ligand L^1H_3 (0.343 g, 0.5 mmol) was dissolved in degassed THF (15.0 mL), to which KH (0.060 g, 1.5 mmol) was added. The mixture was stirred overnight until all KH was dissolved. Pink-colored $CrCl_3$ (0.079 g, 0.5 mmol) was added to this yellow solution as solid and the mixture was allowed to stir overnight to afford a dark brown solution. This solution was evaporated to dryness under vacuum, and the residue was extracted with hexane and filtered. The extract was allowed to stand at room temperature to give dark-brown, needle-like crystals of **4** (0.120 g, 28%). UV−vis (THF): λ_{max} (ε (M^{-1} cm^{-1})) 450 (5380), 500 (4080), 630 (3025). Elemental Analysis: Calcd. for $C_{52}H_{59}ClCrN_4O$ (**4**−$0.75C_6H_{14}$): C, 74.04; H, 7.05; N, 6.64. Found: C, 74.57; H, 7.01; N, 6.69.

$[(L^1)Cr(III)\text{-}THF]$ (5). Ligand L^1H_3 (0.343 g, 0.5 mmol) was dissolved in degassed THF (15.0 mL), to which KH (0.060 g, 1.5 mmol) was added. The mixture was stirred overnight until all KH was dissolved. $CrCl_3$ (0.079 g, 0.5 mmol) was added to this yellow solution as solid, and the solution was allowed to stir overnight to give a dark brown solution. This solution was evaporated to dryness under vacuum, and the residue was extracted with hexane several times and filtered to remove as much of **4** as possible. Once the extracts started to become pale and almost transparent, the remaining residue was extracted with diethyl ether to give a dark green solution. This solution was allowed to stand at room temperature to give dark-green, diamond-shaped crystals of **5** (0.120 g, 30%), which are also air sensitive. UV−vis (THF): λ_{max} (ε (M^{-1} cm^{-1})) 430 (5760), 660 (3700), 800 (sh). Elemental Analysis: Calcd. for $C_{52}H_{59}CrN_4O$ (**5**): C, 77.29; H, 7.36; N, 6.93. Found: C, 76.89; H, 7.12; N, 6.72.

Other Physical Measurements. Cyclic voltammetry was carried out with a Bipotentiostat AFCBP1 from Pine Instrument Company fitted in a Dry Box and controlled with the PineChem 2.7.9 software. Cyclic voltammetry was performed using a gold disk working electrode (1.6 mm diameter) and a Ag/Ag^+ (0.01 M $AgNO_3$ and 0.5 M $[(n\text{-}Bu)_4N]PF_6$ in acetonitrile) nonaqueous reference electrode (Bioanalytical Systems, Inc.) with a prolonged bridge (0.5 M $[(n\text{-}Bu)_4N]PF_6$ in acetonitrile). A thin Pt foil or gauge (8 cm^2, Sigma-Aldrich) was employed as counter electrode. The working electrode was polished using successively 6, 3, 1 μm diamond paste on a DP-Nap polishing cloth (Struers, Westlake, OH), washed with water, acetone and air-dried. The Pt foil and gauge electrodes were cleaned in a H_2O_2/H_2SO_4(conc) solution (1:4 v:v) and oven-dried. The concentration of the samples was 3 mM and that of $[(n\text{-}Bu)_4N]PF_6$ (supporting electrolyte) was 0.5 M. The potential sweep rate varied between 10−1000 mV/s. Unless stated otherwise, all potentials are reported versus the ferrocenium/ferrocene (Fc^+/Fc) couple.

Magnetic susceptibility data were obtained at the Materials Science Department of MIT on a Quantum Design AC MRMS-5S SQUID magnetosusceptometer equipped with a 5.5 T magnet. Data were collected in the temperature range 2−300 K at a field of 1.0 T within the linear response of the magnetic moment vs field relationship. Compound **2** (0.0152 g) was charged in a capsule, which was suspended in a straw. Corrections were made by recording magnetic susceptibility vs temperature data of a blank sample (capsule/straw) and for the diamagnetic contributions with the assistance of Pascal tables.

Crystallographic data were collected at the Department of Chemistry and Chemical Biology at Harvard University by using a Bruker SMART CCD (charge coupled device) based diffractometer equipped with an Oxford Cryostream low-temperature apparatus operating at variable low temperatures. A suitable crystal was chosen and mounted on a glass fiber using grease. Data were measured using omega scans of 0.3° per frame for 30 s, such that a hemisphere was collected. A total of 1271 frames were collected with a maximum resolution of 0.75 Å. The first 50 frames were recollected at the end of data collection to monitor for decay. Cell parameters were retrieved using SMART software and refined using SAINT on all observed reflections. Data reduction was performed using the SAINT software, which corrects for Lp and decay. The structures are solved by the direct method using the SHELXS-97 program and refined by least-squares method on F^2, SHELXL-97, incorporated in SHELXTL-PC V 5.10. All non-hydrogen atoms

Table 1. Summary of Crystallographic Data for Compounds **1**−**5**

	1b	2	3	4	5
formula	$C_{88}H_{103}MnN_4O_4P$	$C_{110}H_{136}K_2Mn_2N_8O_4$	$C_{104}H_{120}N_8O_2$	$C_{56.50}H_{69.50}ClCrN_4O$	$C_{52}H_{59}CrN_4O$
M_r	1366.65	1822.35	1514.08	908.11	808.03
crystal system	monoclinic	triclinic	monoclinic	triclinic	triclinic
space group	$P2(1)/n$	$P\bar{1}$	$C2/c$	$P\bar{1}$	$P\bar{1}$
a (Å)	10.7305(12)	12.6764(17)	39.025(8)	10.4052(6)	11.691(2)
b (Å)	24.248(3)	13.4406(18)	12.187(2)	16.2284(10)	13.995(3)
c (Å)	29.792(3)	16.108(2)	22.221(4)	16.2419(10)	15.370(3)
α (deg)	90	79.940(3)	90.00	81.0380(10)	62.987(3)
β (deg)	98.768(2)	67.018(3)	122.573(4)	83.8510(10)	85.304(4)
γ (deg)	90	83.947(3)	90.00	75.6920(10)	84.835(4)
V (Å^3)	7661.0(15)	2485.7(6)	8906(3)	2618.3(3)	2228.9(7)
Z	4	1	4	2	2
D_{calcd} (g cm^{-3})	1.185	1.217	1.129	1.152	1.204
T (K)	293(2)	99(2)	193(2)	293(2)	213(2)
λ (Å)	0.71073	0.71073	0.71073	0.71073	0.71073
μ (mm^{-1})	0.246	0.393	0.067	0.310	0.298
$R_1{}^a$ (4σ data)	0.1113	0.0778	0.1683	0.1417	0.1942
$wR_2{}^b$ (4σ data)	0.1849	0.1441	0.2538	0.1823	0.1569

^{a} $R_1 = \Sigma||F_o| - |F_c||/\Sigma|F_o|$. ^{b} $wR_2 = [\Sigma w(F_o^2 - F_c^2)^2/\Sigma w(F_o^2)^2]^{1/2}$.

Scheme 1

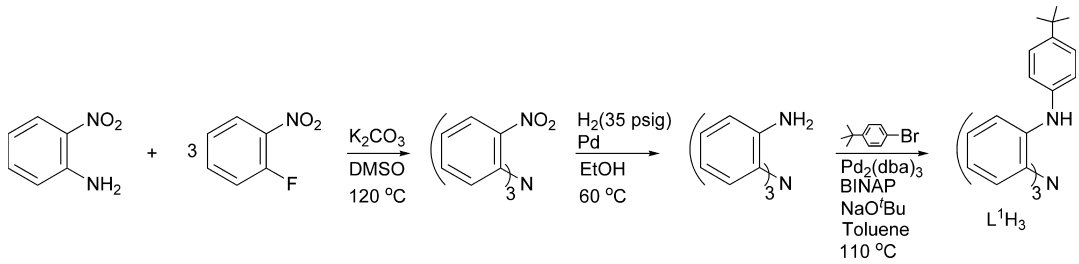

were refined anisotropically. Hydrogens were calculated by geometrical methods and refined as a riding model. The crystals used for diffraction studies showed no decomposition during data collection. All drawings are done at 50% ellipsoids unless otherwise stated. Pertinent crystallographic data are collected in Table 1.

Results and Discussion

Ligand Synthesis. Scheme 1 summarizes the key steps leading to the synthesis of the tripodal trisamido amine ligand L^1H_3. The synthetic protocol relies on the preparation of 2,2′,2″-triaminotriphenylamine,[9] which is further functionalized by virtue of Pd-catalyzed Hartwig-Buchwald arylation of amines. A family of ligands has thus been generated, which can provide a tetradentate C_3-symmetric environment for metallation purposes. Details on the synthesis and characterization of this ligand family have already been published.[9] Here we concentrate on aspects of oxidative reactivity involving Mn(II) and Cr(III) precursor species featuring the prototypical L^1H_3 ligand, in which both metal and ligand are engaged in redox transformations.

Synthesis of Mn(II) Precursor Complexes. The reaction of anhydrous $MnCl_2$ (beads, 99.99%) with 3 equiv of K_3L^1, prepared in situ by deprotonation of the ligand L^1H_3 with KH in THF, leads to generation of yellow-orange solutions from which crystals of $[(L^1)Mn(II)\text{-}THF][K(THF)_x]$ (**1a**) are isolated either from concentrated THF solutions or upon layering pentane over THF solutions of **1a**. The compound is exceedingly air-sensitive (see below) and also loses solvent easily, thus hampering efforts to further define its stoichiometry. The closest analogues are the corresponding iron(II) compounds $[(L^1)Fe(II)\text{-}THF][K(THF)_3]$[8] and $[(L^3)Fe(II)\text{-}THF][K(THF)_2]$,[10] and the Mn(II) compounds $[(L^3)Mn(II)\text{-}THF][K(THF)_2]$ and $[(L^5)Mn(II)\text{-}THF][K(THF)_4]$,[10] where L^3 and L^5 are the 3,5-$(CF_3)_2$ and 3,5-Cl_2 substituted ligands, respectively, in lieu of the 4-*t*-Bu substitution in L^1.

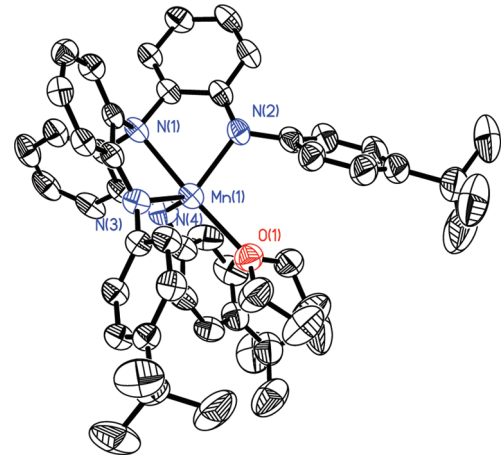

Figure 1. Solid-state structure of $[(L^1)Mn(II)\text{-}THF](Ph_4P)\cdot 3THF$ (**1b**) showing 50% probability ellipsoids and the atom labeling scheme (the countercation $(Ph_4P)^+$ and the solvated THF molecules have been omitted for clarity). Selected interatomic distances (Å) and angles (deg): Mn(1)−N(3) 2.084(3), Mn(1)−N(4) 2.088(3), Mn(1)−N(2) 2.113(3), Mn(1)−O(1) 2.228(3), Mn(1)−N(1) 2.316(3), N(3)−Mn(1)−N(4) 114.92(12), N(3)−Mn(1)−N(2) 115.19(11), N(4)−Mn(1)−N(2) 114.68(12), N(3)−Mn(1)−O(1) 109.57(11), N(4)−Mn(1)−O(1) 99.73(11), N(2)−Mn(1)−O(1) 100.23(11), N(3)−Mn(1)−N(1) 76.91(10), N(4)−Mn(1)−N(1) 77.03(11), N(2)−Mn(1)−N(1) 76.39(10).

Scheme 2

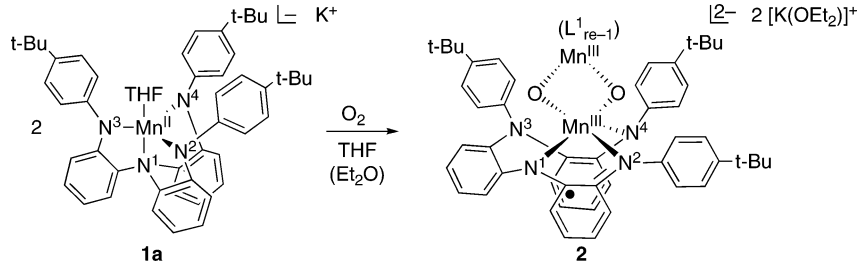

Addition of excess $(Ph_4P)Cl$ to yellow-orange solutions of **1a** in THF affords bright orange solutions from which crystals of $[(L^1)Mn(II)\text{-}THF](Ph_4P)\cdot 3THF$ (**1b**) can be isolated in good yields upon layering with hexane.

The structure of **1b** reveals a distorted trigonal bipyramidal geometry around the Mn(II) site, featuring two similar and a slightly longer $Mn(II)-N_{amido}$ bonds with an average value of 2.095 (3) Å, whereas the $Mn(II)-N_{amine}$ bond is significantly longer at 2.316(3) Å. The distortion is also exemplified by the position of the Mn(II) atom at a distance of 0.479 Å from the plane defined by the three amido nitrogen atoms and toward the coordinated THF molecule, generating an average $N_{amine}-Mn-N_{amido}$ angle of 76.78° consistent with the geometric requirements of five-member rings. All metrical parameters associated with the bond distances noted above are longer by comparison to those found in the analogous Fe(II) complex,[8] reflecting the larger ionic radius of Mn(II).

The dual mode X-band EPR spectrum of **1a** in frozen THF (5 mM) (Figure S1 in the Supporting Information and Figure 5 below) consists of signals in a wide field region in the perpendicular mode (g = 14.7, 5.10, 3.21, 2.06) and a characteristic signal in parallel mode. Both are very similar to those previously observed for mononuclear Mn(II) complexes,[11] albeit slightly shifted. The axial component of the zero-field splitting parameter $|D|$ (on the order of 0.1 cm^{-1} for **1a**) and the rhombicity ($E/D \sim 0.15-0.25$) are also similar to reported values.

Oxidation of Mn(II) Precursor with Dioxygen. Yellow-orange solutions of $[(L^1)Mn(II)\text{-}THF][K(THF)_x]$ in THF are exceedingly sensitive to dry dioxygen, turning green-brown instantaneously upon quick exposure (1−3 min). Exhaustive extraction with hexane and crystallization from Et_2O/hexane provides dark green-brown crystals of $[(L^1_{re-1})Mn(III)\text{-}(O)_2\text{-}Mn(III)(L^1_{re-1})][K(OEt_2)]_2\cdot C_6H_{14}$ (**2**). Following extraction with hexane, a small amount of a remaining brown compound can be obtained from diethyl ether extracts. Despite numerous attempts, the brown species has not provided suitable crystalline samples and remains as yet uncharacterized. However, glimpses to its possible nature are discussed in subsequent sections.

Compound **2** features a ligand that has been rearranged with respect to the intact C_3-symmetric ligand of **1**. As indicated below, the ligand reorganization is triggered by a one-electron oxidation, followed by migration of a phenylene ring (bridging between atoms N^1 and N^4) from atom N^1 to atom N^3 (Scheme 2). Furthermore, the oxidizing equivalent that initiates this radical 1,4-(*N*-to-*N*) phenyl migration[12] is retained as a radical site on a newly formed *o*-diiminosemibenzoquinonate (*o*-disq$^-$) moiety.[13]

The ligand rearrangement compromises the integrity of the C_3-symmetric ligand and alleviates the steric hindrance imposed by the three 4-*t*-butyl-phenyl arms. As a consequence, the structure of compound **2** is dimeric (Figure 2), featuring a $Mn(\mu\text{-}O)_2Mn$ core at the rare Mn(III) oxidation level, and a radical-containing ligand (S = 1/2) per Mn. The coordination of the asymmetric core of the centrosymmetric structure of **2** is best viewed in Figure 3. Each Mn(III) site possesses a distorted trigonal bipyramidal coordination geometry, defined with respect to Mn(1) by the equatorial atoms O(1A), N(2) and N(4) and the axial atoms N(1) and O(1) (N(1)−Mn(1)−O(1) = 164.38(7)°). The position assignment of the symmetry related O and O(1A) atoms reverses for Mn(1A). The purely amine-type atoms N(3) and N(3A) lie outside the coordination sphere of Mn(1) and Mn(1A), respectively (Mn(1)−N(3) = 3.417 Å). The elongation of the Mn(1)−N(4) bond (2.1270(18) Å) associated with this genuine N_{amido} atom is most likely due to the Jahn−Teller effect, which is typical of Mn(III), d^4 sites, and its axis tends to lie perpendicular to the planar Mn_2O_2 core. The semiimino nature of atoms N(1) and N(2) associated with the *o*-disq$^-$ moiety is supported by the average C−N bond distance (1.375(3) Å) that lies between a single and a double bond, the pattern of four long and two short C−C bonds, as well as the longer than expected Mn−N bond distances for genuine N_{amido} atoms (Mn(1)−N(1) = 2.0311(19), Mn(1)−N(2) = 2.0114(18) Å).

Metrical parameters for the $Mn(III)(O)_2Mn(III)$ core of all isolable compounds known to date are collected in Table 2.[14−20] Compound **2** possesses the longest Mn−Mn distance and one of the longest Mn−O−Mn angles, possibly reflecting

(10) Pinnapareddy, D.; Paraskevopoulou, P.; Stavropoulos. P., manuscript in preparation.
(11) Pierce, B. S.; Elgren, T. E.; Hendrich, M. P. *J. Am. Chem. Soc.* **2003**, *125*, 8748–8759.
(12) Studer, A.; Bossart, M. *Tetrahedron* **2001**, *57*, 9649–9667.
(13) (a) Herebian, D.; Wieghardt, K. E.; Neese, F. *J. Am. Chem. Soc.* **2003**, *125*, 10997–11005. (b) Chaudhuri, P.; Verani, C. N.; Bill, E.; Bothe, E.; Weyhermüller, T.; Wieghardt, K. *J. Am. Chem. Soc.* **2001**, *123*, 2213–2223.
(14) Gultneh, Y.; Yisgedu, T. B.; Tesema, Y. T.; Butcher, R. J. *Inorg. Chem.* **2003**, *42*, 1857–1867.
(15) Mikata, Y.; So, H.; Yamashita, A.; Kawamura, A.; Mikuriya, M.; Fukui, K.; Ichimura, A.; Yano, S. *Dalton Trans.* **2007**, 3330–3334.
(16) Goodson, P. A.; Oki, A. R.; Glerup, J.; Hodgson, D. J. *J. Am. Chem. Soc.* **1990**, *112*, 6248–6254.
(17) Goodson, P. A.; Hodgson, D. J. *Inorg. Chem.* **1989**, *28*, 3606–3608.
(18) Kitajima, N.; Singh, U. P.; Amagai, H.; Osawa, M.; Moro-oka, Y. *J. Am. Chem. Soc.* **1991**, *113*, 7757–7758.

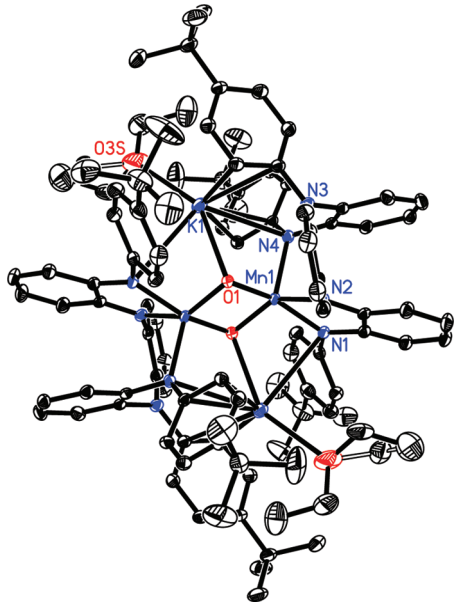

Figure 2. Solid-state structure of $[(L^{1}_{re-1})Mn(III)\text{-}(O)_2\text{-}Mn(III)\text{-}(L^{1}_{re-1})][K(OEt_2)]_2 \cdot C_6H_{14}$ (**2**) showing 50% probability ellipsoids and the atom labeling scheme. Selected interatomic distances (Å) and angles (deg) are Mn(1)−O(1) 1.8328(15), Mn(1)−O(1A) 1.8592(15), Mn(1)−N(2) 2.0114(18), Mn(1)−N(1) 2.0311(19), Mn(1)−N(4) 2.1270(18), O(1)−Mn(1)−O(1A) 84.30(7), K(1)−O(1) 2.6932(16), K(1)−O(3S) 2.748(2), Mn(1)−O(1)−Mn(1A) 95.70(7), O(1)−Mn(1)−N(2) 95.63(7), O(1A)−Mn(1)−N(2) 142.82(7), O(1)−Mn(1)−N(1) 164.38(7), O(1A)−Mn(1)−N(1) 91.41(7), N(2)−Mn(1)−N(1) 78.77(7), O(1)−Mn(1)−N(4) 97.98(7), O(1A)−Mn(1)−N(4) 117.00(7), N(2)−Mn(1)−N(4) 99.89(7), N(1)−Mn(1)−N(4) 97.35(7), O(1)−Mn(1)−Mn(1A) 42.52(5), O(1A)−Mn(1)−Mn(1A) 41.78(5), N(2)−Mn(1)−Mn(1A) 127.36(5), N(1)−Mn(1)−Mn(1A) 131.42(6), N(4)−Mn(1)−Mn(1A) 113.66(5).

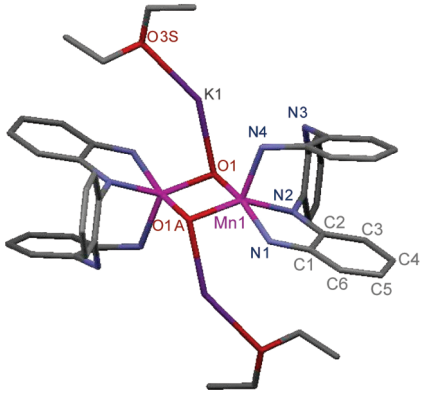

Figure 3. Detail of the solid-state structure of **2** showing the $Mn(O)_2Mn$ core and the first coordination sphere. Bond distances (Å) related to the *o*-disq$^-$ moiety are as follows: N(1)−C(1) 1.362(3), N(2)−C(2) 1.352(3), C(1)−C(2) 1.441(3), C(2)−C(3) 1.425(3), C(3)−C(4) 1.370(3), C(4)−C(5) 1.412(4), C(5)−C(6) 1.374(3), C(6)−C(1) 1.419(3).

the steric encumbrance around each Mn(III) site. Otherwise, the Mn−O bond distances of **2** are within the range expected for Mn(III) and, on average, longer than those known for the much more common mixed-valent $Mn(III)(O)_2Mn(IV)$ and $Mn(IV)(O)_2Mn(IV)$ cores.[6] Presumambly, the $Mn(III)\text{-}(O)_2Mn(III)$ core is stabilized in **2** due to the weaker ligand field imposed by the semiimino N atoms and the non-coordination of the N_{amine} atom as a result of steric hindrance. It is worthwhile noting that each potassium ion makes close contact to one of the oxo bridges as shown in Scheme 2, and is further supported by a diethyl ether molecule and several electron-rich aromatic carbons and nitrogen atoms that are within van der Waals distance.[21]

The stretching vibrations of the Mn−O bonds associated with the $Mn(O)_2Mn$ core are obscured by a broad ligand-derived absorption band, but a difference spectrum with respect to the ligand as well as the analogous $[(L^{1}_{re-1})Fe(III)\text{-}O\text{-}Fe(III)(L^{1}_{re-1})]$ complex,[8] reveals that a residual band at 730 cm^{-1} can be tentatively assigned to the stretching of the $Mn(O)_2Mn$ core (Figure S2 in the Supporting Information). This is at slightly higher wavenumber than the reported range (670−700 cm^{-1}) for similar compounds containing the $Mn(O)_2Mn$ core.

A similar diferric μ-oxo compound ($[(L^{1}_{re-1})Fe(III)\text{-}O\text{-}Fe(III)(L^{1}_{re-1})]$) carrying the same oxidatively rearranged ligand has been previously isolated.[8] The iron congener is distinguished with respect to **2** by virtue of a single oxo bridge, a close Fe−N_{amine} contact (2.458(4) Å) and a strong Fe−N_{amido} bond (1.960(5) Å). These features stabilize the iron compound with respect to further oxidation by dioxygen, whereas compound **2** evolves further upon prolonged exposure to dioxygen (see below).

Magnetics. Magnetic susceptibility data for compound **2** were collected in the temperature range 5−300 K at a field strength of 1.0 T, and were corrected for the magnetization of the sample holder. The measured molar magnetic susceptibility for **2** as a function of temperature is shown in Figure 4. The product $\chi_M T$, where χ_M is the molar susceptibility, decreases with decreasing temperature. The spin Hamiltonian and the expression used to fit the susceptibility data in the temperature range 10−300 K are given in eqs 1 and 2, where $S_1 = S_4 = 1/2$ (ligand radical) and $S_2 = S_3 = 2$ (Mn(III)) and ρ is the paramagnetic impurity of a Mn(III) ion. The expression (eq 2) used to fit the magnetic susceptibility data incorporates the contribution of the molar susceptibility of compound **2** as determined from the Hamiltonian (first term of eq 2) plus the contribution of a fraction ρ of paramagnetic impurities due to a Mn(III) ion according to the Curie law (second term of eq 2).[22] The best fit is shown in the same figure as a solid line and corresponds to $g = 2.0$ (fixed), $J_{R\text{-}Mn} > -600$ cm^{-1} (undefined) for the coupling between each Mn(III) and ligand-centered radical, and $J_{Mn-Mn} = -120(3)$ cm^{-1} for the coupling between the two Mn(III) via the oxo bridges and $\rho = 3.3\%$. Although an $S = 0$ ground-state is expected, the nonzero susceptibility at low temperatures is due to a paramagnetic impurity of a manganese ion. The more drastic decrease below 8 K is due to zero-field effects of this impurity. It was not possible to

(19) Glerup, J.; Goodson, P. A.; Hazell, A.; Hazell, R.; Hodgson, D. J.; McKenzie, C. J.; Michelsen, K.; Rychlewska, U.; Toftlund, H. *Inorg. Chem.* **1994**, *33*, 4105–4111.
(20) Hitomi, Y.; o, A.; Matsui, H.; Ito, T.; Tanaka, T.; Ogo, S.; Funabiki, T. *Inorg. Chem.* **2005**, *44*, 3473–3478.
(21) (a) Huffman, J. C.; Green, M. A.; Kaiser, S. L.; Caulton, K. G. *J. Am. Chem. Soc.* **1985**, *107*, 5111–5115. (b) Bouwkamp, M. W.; Lobkovsky, E.; Chirik, P. J. *Inorg. Chem.* **2006**, *45*, 2–4.
(22) (a) Kahn, O. *Molecular Magnetism*; VCH Publishers: New York, 1993. (b) Andersen, N. H.; Døssing, A.; Mølgaard, A. *Inorg. Chem.* **2003**, *42*, 6050–6055.

Table 2. Physicochemical Parameters of the Mn(III)-$(O)_2$-Mn(III) Core[a]

compound	Mn···Mn (Å)	Mn−O(1) (Å)	Mn−O(2) (Å)	Mn−O−Mn (deg)	O(1)−Mn−O(2) (deg)	J (cm^{-1})	$E(Mn_2^{III,III}/Mn_2^{III,IV})$, $E(Mn_2^{III,IV}/Mn_2^{IV,IV})$ (V vs Ag/AgCl)	ref
$[L^2MnO]_2(ClO_4)_2\cdot H_2O$	2.676(3)	1.814(8)	1.853(9)	94.5(4)	86.3(4)	−86.4 ± 0.2	0.568, 1.337	16
		1.830(9)	1.863(8)	92.1(4)	87.1(4)			
$[L^3MnO]_2(NO_3)_2\cdot 6H_2O$	2.674(4)	1.818(9)	1.841(6)	93.9(3)	86.1(3)		0.678, 1.446	15
$[L^3MnO]_2(ClO_4)_2$								15
$[L^4MnO]_2(ClO_4)_3$							0.090, 0.903	15
$[L^5MnO]_2(ClO_4)_2\cdot 7H_2O$	2.686(1)	1.855(4)	1.851(4)	93.3(2)	85.7(2)		no electrochemistry in the region of −0.5 − (+1.8) V	15
		1.839(4)	1.824(4)	93.9(2)	87.0(2)			
$[L^6MnO]_2$	2.696(2)	1.806(5)	1.813(6)	96.5(3)		2.81 μ_B/mol		17
		1.808(6)	1.787(6)	97.0(3)				
$[L^7MnO]_2(ClO_4)_2\cdot 5H_2O$	2.699(2)	1.846(4)	1.851(4)	93.8(2)	86.2(2)	−101(1)		18
$[L^8MnO]_2(ClO_4)_2$	2.7042(5)	1.8264(12)	1.8285(12)	95.44(6)	84.56(6)		0.87, 1.70	13
$[L^9MnO]_2(ClO_4)_2\cdot 2.2MeCN$	2.7067(11)	1.822(3)	1.830(2)	95.67(12)	84.33(12)		0.78, 1.58	13
	2.7119(12)	1.826(3)	1.829(3)	95.80(12)	84.20(12)			
$[L^{10}MnO]_2(ClO_4)_2\cdot 2DMF$	2.6649(5)	1.8238(19)	1.8251(19)	93.83(9)	86.15(8)	−97.5	0.79, 1.61	14
$[L^{11}MnO]_2(ClO_4)_2\cdot H_2O$	2.6675(9)	1.824(2)	1.821(2)	93.77(11)	86.34(12)	−82.9	0.80, 1.64	14
		1.830(2)	1.828(2)	93.92(11)	85.96(12)			
$[L^{12}MnO]_2(BPh_4)_2$	2.656(2)	1.866(3)	1.861(3)	90.9(1)	89.1(1)			19
$[(L^1_{re-1})MnO]_2[K(OEt_2)]_2\cdot C_6H_{14}$ (**2**)	2.7373(7)	1.8328(15)	1.8592(15)	95.70(7)	84.30(7)	−120	see text	this work

[a] L^2: *N*,*N*′-bis((6-methylpyrid-2-yl)methyl)ethane-1,2-diamine; L^3: *N*,*N*′-bis((6-methylpyrid-2-yl)methyl)-*N*-2-pyridylmethylamine; L^4: *N*,*N*′-bis((4-methylpyrid-2-yl)methyl)ethane-1,2-diamine; L^5: *N*,*N*′-bis(2-methylpyrazyl)ethane-1,2-diamine; L^6: hydrotris(3,5-diisopropyl-1-pyrazolyl)borate; L^7: *N*,*N*′-bis(2-pyridylmethyl)-*N*,*N*′-dimethyl-1,2-ethanediamine; L^8: tris(6-methyl-2-pyridylmethyl)diamine; L^9: 2-(2-pyridyl)ethylbis(6-methyl-2-pyridylmethyl)amine; L^{10}: *N*,*N*′-bis(2-quinolylmethyl)-*N*,*N*′-dimethyl-1,2-ethanediamine; L^{11}: N,*N*′-bis(2-quinolylmethyl)-*N*,*N*′-diethyl-1,2-ethanediamine; L^{12}: tris(pyrid-2-ylmethyl)-amine.

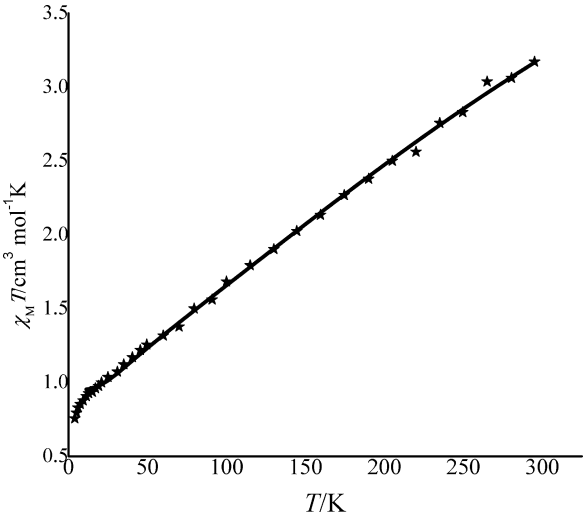

Figure 4. Temperature dependence of the susceptibility data of compound **2** in the form of $\chi_M T$ vs T (solid stars) along with the fitting results (solid line) according to eqs 1 and 2. See text for details.

simulate this parameter from the above fitting procedure since the above model will be overparametrized.

$$H_{exc} = -2J_{R-Mn}(S_1\cdot S_2 + S_3\cdot S_4) - 2J_{Mn-Mn}(S_2\cdot S_3) + \sum_{i=1}^{4}\mu_B B\cdot g_i\cdot S_i \quad (1)$$

$$\chi = (1-\rho)\chi_{exc} + \rho\frac{Ng^2\mu_B^2 S(S+1)}{3\kappa_B T} \quad (2)$$

The magnetic susceptibility data of $[(L^1_{re-1})Fe(III)-O-Fe(III)(L^1_{re-1})]$ show a similar trend to that observed with **2**, featuring a strong antiferromagnetic coupling between the metal and the ligand-based radical ($J_{R\text{-}Fe} > -500$ cm^{-1} (undefined)) and a more modest antiferromagnetic coupling between the two metals ($J_{Fe-Fe} = -123$ cm^{-1}). The value of J_{Mn-Mn} for **2** is somewhat larger than that reported for other [Mn(III)$(O)_2$Mn(III)]-containing compounds,[14−20] but the available data remain limited for any meaningful magneto-structural correlations[23] (Table 2). The related $[Mn_2(5\text{-}MeOsaltmen)_2(DCNNQI)_2]$ compound[24] (5-MeOsaltmen^{2-} = *N*,*N*′-(1,1,2,2-tetramethylethylene)bis(5-methoxysalicylideneiminate); DCNNQI = *N*,*N*-dicyano-1,4-naphthoquinonediiminate radical), which features two phenolate bridges, exhibits strong antiferromagnetic coupling between the Mn(III) ion and the ligand-residing radical, but weak ferromagnetic Mn(III)/Mn(III) coupling via the phenolate bridges.

Other Species in the Reaction of Mn(II) and Dioxygen. The progression of the reaction of THF solutions of **1a** (5 mM) with dry dioxygen was monitored by X-band EPR spectroscopy. At certain time intervals batches of samples (∼200 μL) were removed, transferred to EPR tubes and plunged into liquid nitrogen. Interaction with O_2 for approximately 0.5 min leads to the disappearance of the Mn(II) signal noted above. At 4.2 K, the loss of the feature at g ∼ 5.1 from the Mn(II) monomer signal is accompanied by the appearance of a new signal of different shape consisting of a relatively broad absorption with an apparent peak at roughly the same g-value (Figure 5, left). Its temperature dependence suggests that it arises from a ground spin state. This feature is consistent with an $S = 3/2$ system with a zero-field splitting parameter $|D| \gg h\nu$(∼0.3 cm^{-1} at X-band) and rhombic distortion ($E/D \sim 0.2$). Such an $S = 3/2$ derived signal has been observed in mononuclear Mn(IV)

(23) Law, N. A.; Kampf, J. W.; Pecoraro, V. L. *Inorg. Chim. Acta* **2000**, *297*, 252–264.
(24) Kachi-Terajima, C.; Miyasaka, H.; Sugiura, K.-I.; Clérac, R.; Nojiri, H. *Inorg. Chem.* **2006**, *45*, 4381–4390.

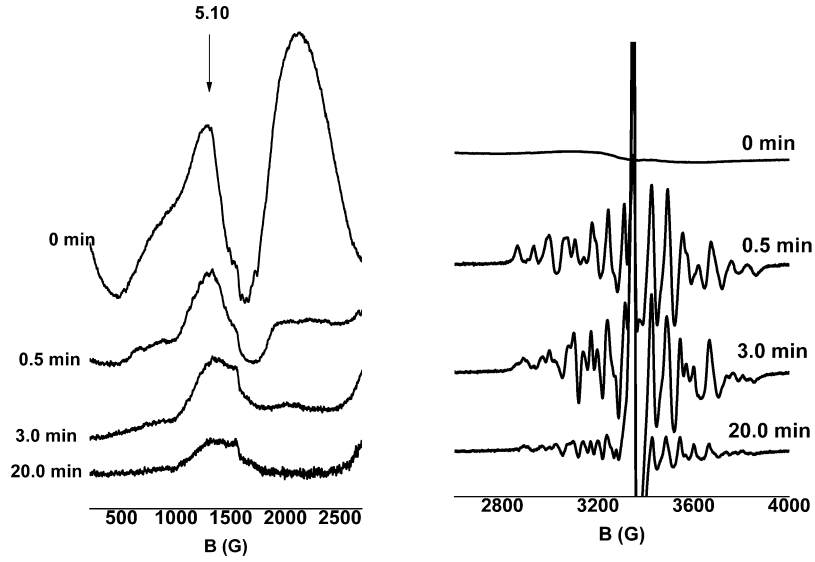

Figure 5. Perpendicular mode X-band EPR spectra of a 5 mM solution of [(L^1)Mn(II)-THF][K(THF)$_x$] (**1a**) in THF after exposure to dioxygen for 0, 0.5, 3.0, and 20 min. EPR parameters: (Left) $T = 4.2$ K, microwave power 2.2 mW, modulation amplitude 25 Gpp, microwave frequency 9.42 GHz; (Right) $T = 4.2$ K, microwave power 0.15 mW, modulation amplitude 5 Gpp, microwave frequency 9.42 GHz.

complexes,[25] but may also arise from strong antiferromagnetic coupling between a Mn(III) ion ($S = 2$) and an $S = 1/2$ radical-bearing moiety, or between a Mn(II) ion ($S = 5/2$) and two $S = 1/2$ radical residues.[26] Electrochemical data (see below) favor the Mn(III)-L$^{\bullet}$ scenario.

A second feature that grows in as the Mn(II) signal disappears is a multiline signal at $g = 2.0$ (Figure 5, right). The general appearance of the signal is that of a pseudo 16-line spectrum,[27] which is strongly reminiscent of the signals observed from Mn(III)−Mn(IV) dimers. The temperature dependence indicates that the spin state responsible for this signal is an $S = 1/2$ ground state, well isolated from other spin manifolds of the coupled system, implying strong exchange coupling. That the ground-state is well-isolated from other spin states (as the result of strong exchange coupling) is further supported by the slow relaxation properties of the signal at 4.2 K as suggested by its facile saturation. Such a property is generally observed in mono- or dioxo bridged Mn(III)−Mn(IV) dimers as opposed to relevant Mn(II)−Mn(III) dimers.[28] However, the width of the observed signal (∼1000 G) is narrower than that reported for mono-oxo or dioxo-bridged Mn(III)−Mn(IV) compounds (∼1190 and 1250 G, respectively).[29] Simulations of the spectrum with an $S = 1/2$ system interacting with two ^{55}Mn($I = 5/2$) nuclei indicate anisotropic hyperfine tensors for both ^{55}Mn sites with apparent isotropic values of $A_{1,\mathrm{iso}} \sim 296$ MHz and $A_{2,\mathrm{iso}} \sim 171$ MHz. If we assume a Mn(III)−Mn(IV) dimer, A_1 is consistent with the Mn(III) site and A_2 with the Mn(IV) site, although these values are relatively small by comparison with known examples of mono-oxo or dioxo bridged Mn(III)−Mn(IV) complexes.[29] A possible explanation for these reduced ^{55}Mn hyperfine values is that appreciable spin density delocalizes toward the ligand due to covalency.[29b] It is also conceivable that the signal may be better accommodated by a [Mn(III)−Mn(III)(L$^{\bullet}$)] species, a precursor of the EPR-silent compound **2**.

As the time of interaction of **1a** with O_2 increases to 3.0 min, the $S = 1/2$ multiline signal noted above decreases to ca. 35% of that observed at 0.5 min and at longer times is completely lost. However, a new multiline signal with very similar properties is evident at 3.0 min, which also decays slowly over time (at 20 min only 35% of the intensity observed in the 3.0 min spectrum is observed). This new multiline signal exhibits slow relaxation and comparable width (970 G) with respect to the previous $S = 1/2$ multiline signal, but is more complicated exhibiting more than 16 lines. If we assume an $S = 1/2$ system interacting with two ^{55}Mn($I = 5/2$) nuclei as before, the smaller width suggests smaller values for the hyperfine tensors. This signal is associated with the second minor species isolated from ethereal extracts as noted above, and is again likely to contain a [Mn(III)-Mn(III)(L$^{\bullet}$)] core.

Finally, the decrease of the aforementioned signals is accompanied by the emergence of a relatively narrow ($\Delta H_{\mathrm{pp}} = 12$ G) free-radical signal centered at $g = 2.0048$ (Figure S3 in the Supporting Information, after 20 min interaction with O_2 at room temperature).

Exposing bulk solutions of **1a** (or **2**) in THF to O_2 for 15−20 min results in precipitation of MnO_2 and generation

(25) (a) Kessissoglou, D. P.; Li, X.; Butler, W. M.; Pecoraro, V. *Inorg. Chem.* **1987**, *26*, 2487–2492. (b) Campbell, K. H.; Lashley, M. R.; Wyatt, J. K.; Nantz, M. H.; Britt, R. D. *J. Am. Chem. Soc.* **2001**, *123*, 5710–5719. (c) Hureau, C.; Anxolabéhére-Mallart, E.; Blondin, G.; Riviere, E.; Nierlich, M. *Eur. J. Inorg. Chem.* **2005**, 4808–4817. (d) Parsell, T. H.; Behan, R. K.; Green, M. T.; Hendrich, M. P.; Borovik, A. S. *J. Am. Chem. Soc.* **2006**, *128*, 8728–8729.

(26) Lu, C. C.; Bill, E.; Weyhermüller, T.; Bothe, E.; Wieghardt, K. *J. Am. Chem. Soc.* **2008**, *130*, 3181–3197.

(27) (a) Dismukes, G. C.; Siderer, Y. *Proc. Natl. Acad. Sci. U.S.A.* **1981**, *78*, 274–278. (b) Pessiki, P. J.; Khangulov, S. V.; Ho, D. M.; Dismukes, G. C. *J. Am. Chem. Soc.* **1994**, *116*, 891–897.

(28) Kulik, L. V.; Lubitz, W.; Messinger, J. *Biochemistry* **2005**, *44*, 9368–9374.

(29) (a) Schäfer, K.-O.; Bittl, R.; Lendzian, F.; Barynin, V.; Weyhermüller, T.; Wieghardt, K.; Lubitz, J. *Phys. Chem. B* **2003**, *107*, 1242–1250. (b) Horner, O.; Anxolabéhére-Mallart, E.; Charlot, M.-F.; Tchertanov, L.; Guilhem, J.; Mattioli, T. A.; Boussac, A.; Girerd, J.-J. *Inorg. Chem.* **1999**, *38*, 1222–1232.

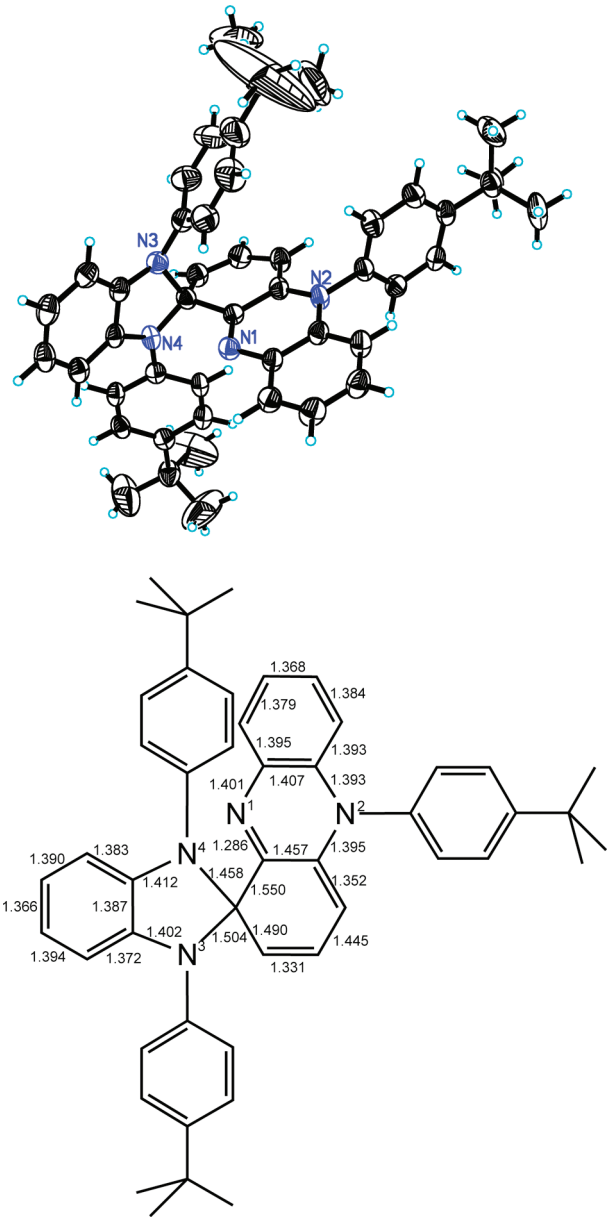

Figure 6. (Top) Solid-state structure of $[L^1_{re\text{-}4}]$ (**3**) showing 50% probability ellipsoids and the atom labeling scheme. (Bottom) Selected interatomic distances (Å).

of a pink solution, from which the diamagnetic, metal-free species $[L^1_{re\text{-}4}]$ (**3**) is isolated as purple crystals from diethyl ether. Its spiro structure (Figure 6) indicates further oxidative rearrangement of the ligand framework (see below for details) although its stoichiometry is the same as that of the deprotonated ligands $[L^1]^{3-}$ or $[L^1_{re\text{-}1}]^{2-}$ minus one hydrogen atom. It can be perceived as the product of a formal four-electron oxidation of $[L^1]^{3-}$ (or three-electron oxidation versus $[L^1_{re\text{-}1}]^{2-}$) according to eq 3. The compound is unstable in solution and slowly gives rise to unidentified $S = 1/2$ radical species as noted by EPR spectroscopy.

$$[L^1]^{3-} \rightarrow [L^1_{re-4}]\ (\mathbf{3}) + 4e^- + H^+ \qquad (3)$$

Electrochemistry. The cyclic voltammogram of **1a** in THF (Figure 7) shows one wave at an $E_{1/2}$ value of −0.228 V (ΔE = 111 mV, $i_{p,a}/i_{p,c}$ = 1.12), most likely due to the Mn(II)/Mn(III) couple, followed by two-electron anodic

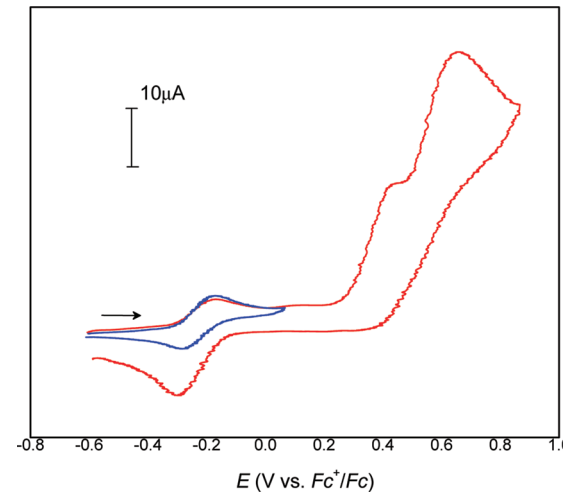

Figure 7. Cyclic voltammogram of $[(L^1)Mn(II)\text{-}THF][K(THF)_x]$ (**1a**) in THF/$[(n\text{-}Bu)_4N]PF_6$ (0.5 M) with a Au disk electrode (1.6 mm in diameter); scan rate 0.1 V/s. Arrow indicates direction of scan.

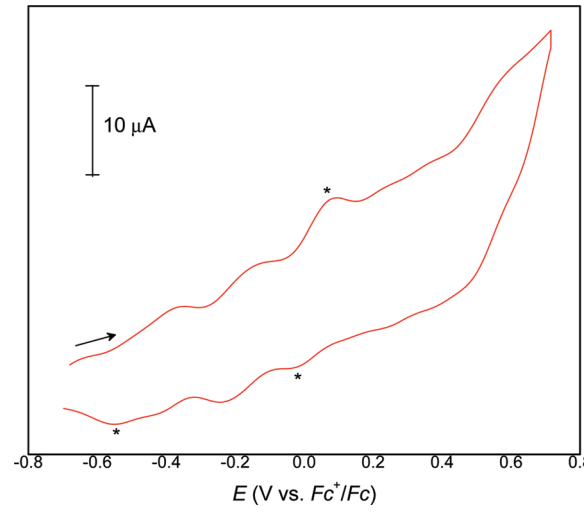

Figure 8. Cyclic voltammogram of $[(L^1_{re-1})Mn(III)\text{-}(O)_2\text{-}Mn(III)\text{-}(L^1_{re-1})][K(OEt_2)]_2$ (**2**) in THF/$[(n\text{-}Bu)_4N]PF_6$ (0.5 M) with a Au disk electrode (1.6 mm in diameter); scan rate 0.1 V/s. Arrow indicates direction of scan.

waves at 0.415 and 0.628 V and a cathodic wave at −0.294 V (vs the Fc^+/Fc couple). Similar behavior has been observed[7] with the electrochemical oxidation of tetrahydrofuran solutions of $[(L^1)Fe(II)\text{-}THF]^-$, albeit at more accessible potentials, and assigned to *independent* one-electron Fe(II)/Fe(III) (quasi-reversible wave) and two-electron (L^1)-Fe(II) → (L^1_{re-1})-Fe(III) (first anodic wave) transformations. It is thus likely that the 0.415 V anodic wave is due to (L^1)-Mn(II) → (L^1_{re-1})-Mn(III) and that the $S = 3/2$ EPR signal which is consistent with a formal Mn(IV) mononuclear site observed by EPR in the early stages of the reaction of Mn(II) with dioxygen may be equivalent to the electrochemically accessible (L^1_{re-1})-Mn(III) species. Furthermore, the presence of both Mn(III) and (L^1_{re-1})-Mn(III) containing sites may be responsible for providing the initial [Mn(III)Mn(III)(L•)] compound as indicated by EPR spectroscopy.

The oxidation of **2** was examined by cyclic voltammetry in THF (Figure 8) and MeCN. In both cases the main feature of the voltammograms are two anodic/cathodic waves at $E_{1/2}$ values of −0.402 (ΔE = 63 mV) and −0.191 (ΔE = 102

Scheme 3

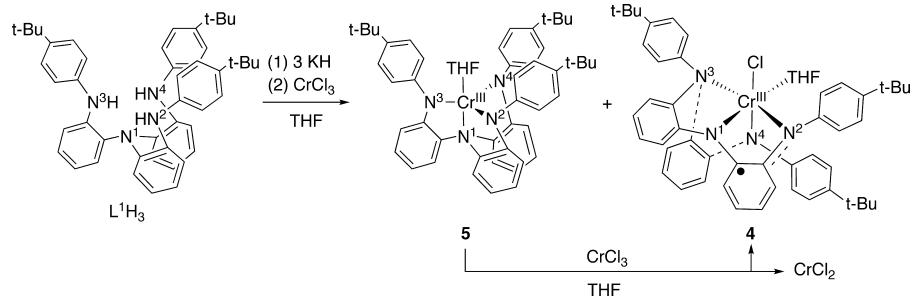

Scheme 4

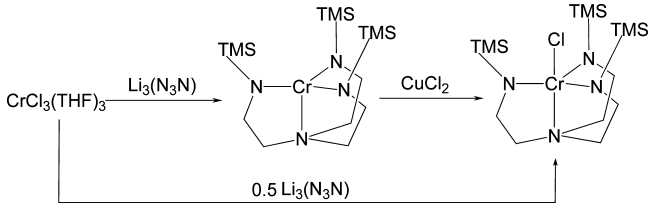

mV) V. It is more likely that those represent ligand-centered rather than metal-centered events, especially since the $E_{1/2}$ values (vs Ag/AgCl)[30] are low with respect to values reported for Mn(III)Mn(III) → Mn(III)Mn(IV) and Mn(III)Mn(IV) → Mn(IV)Mn(IV) couples (Table 2). In addition, an irreversible wave at $E_{p,a} = 0.079$ V and two cathodic waves at −0.018 and −0.547 V are noted (Figure 8, marked with asterisks), which are all dominant features in the cyclic voltammogram of the metal-free species **3** (Figure S4 in the Supporting Information). The intensity of the features associated with **3** increases upon exposure of **2** to dioxygen at the expense of the aforementioned waves at −0.402 and −0.191 V.

Synthesis of Cr(III) Complexes. In order to establish whether the behavior of ligand L^1H_3 with respect to Cr(III) sites is similar to that encountered with Mn(III) complexes, the deprotonated ligand K_3L^1 was reacted with anhydrous $CrCl_3$ in THF to afford dark brown-green solutions. Two air-sensitive products can be isolated from this reaction. Brown hexane extracts afford needle-like crystals of $[(L^1_{re-1})Cr(III)\text{-}(Cl)(THF)]\cdot 0.75C_6H_{14}$ (**4**), whereas the residue can be crystallized from diethyl ether to provide dark green, diamond-shaped crystals of $[(L^1)Cr(III)\text{-}(THF)]$ (**5**). Hence, both the intact and the oxidatively rearranged ligand are featured in **5** and **4**, respectively. The quantitative generation of **4** from **5** in THF according to eq 4 provides an explanation for the formation of both species in the reaction of $L^1{}_3K$ and $CrCl_3$.

$$[(L^1)Cr(III) - (THF)]\ (\mathbf{5}) + CrCl_3 \rightarrow [(L^1_{re-1})Cr(III) - (Cl)(THF)]\ (\mathbf{4}) + CrCl_2 \quad (4)$$

Thus $CrCl_3$ acts both as a ligand metallation source and an oxidizing agent. The first oxidizing equivalent above the Cr(III) level is therefore directed toward the ligand, in sharp contrast to the well-established silyl-derivatized, TREN-containing compound $[Cr(III)(N_3N)]$ which is reportedly oxidized by $CuCl_2$ to $[Cr(IV)(N_3N)Cl]$ (Scheme 4)[31] as well as by other oxidants such as AgX and halogens.[32] The

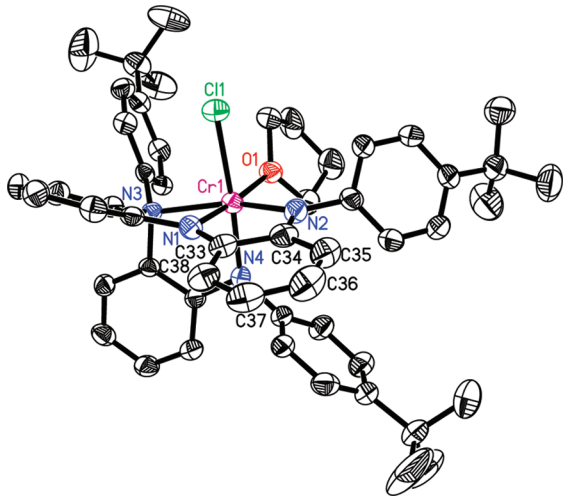

Figure 9. Solid-state structure of $[(L^1_{re-1})Cr(III)\text{-}(Cl)(THF)]\cdot 2C_6H_{14}$ (**4**) showing 50% probability ellipsoids and the atom labeling scheme. Selected interatomic distances (Å) and angles (deg): Cr(1)−N(1) 1.932(4), Cr(1)−N(2) 1.959(4), Cr(1)−N(4) 2.019(4), Cr(1)−O(1) 2.102(3), Cr(1)−N(3) 2.216(3), Cr(1)−Cl(1) 2.3452(13), N(1)−Cr(1)−N(2) 81.19(16), N(1)−Cr(1)−N(4) 94.76(15), N(2)−Cr(1)−N(4) 94.14(15), N(1)−Cr(1)−N(3) 80.63(14), N(2)−Cr(1)−N(3) 160.57(15), N(3)−Cr(1)−N(4) 80.62(13), N(1)−Cr(1)−Cl(1) 88.70(11), N(2)−Cr(1)−Cl(1) 92.97(11), N(3)−Cr(1)−Cl(1) 93.41(9), N(4)−Cr(1)−Cl(1) 172.50(12), N(1)−Cr(1)−O(1) 175.31(14).

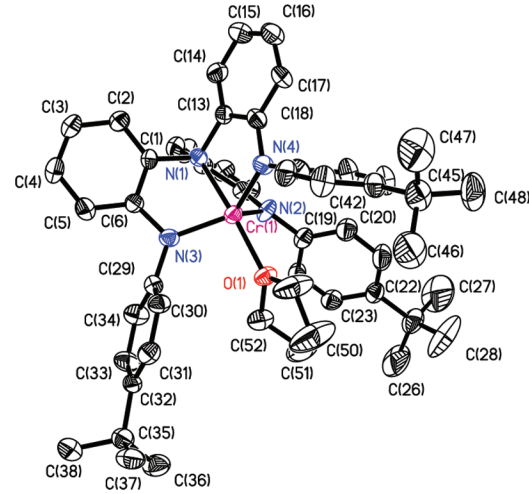

Figure 10. Solid-state structure of $[(L^1)Cr(III)\text{-}THF]$ (**5**) showing 50% probability ellipsoids and the atom labeling scheme. Selected interatomic distances (Å) and angles (deg): Cr(1)−N(1) 2.094(3), Cr(1)−N(2) 1.969(3), Cr(1)−N(3) 1.943(3), Cr(1)−N(4) 1.965(3), N(1)−C(13) 1.474(5), N(1)−C(1) 1.479(4), N(1)−C(7) 1.486(4), N(2)−C(12) 1.373(5), N(2)−C(19) 1.427(5), N(3)−C(6) 1.398(4), N(3)−C(29) 1.439(5), N(4)−C(18) 1.397(4), N(4)−C(39) 1.423(5), N(3)−Cr(1)−N(4) 124.20(13), N(3)−Cr(1)−N(2) 125.96(14), N(4)−Cr(1)−N(2) 104.34(14), N(3)−Cr(1)−O(1) 94.95(12), N(4)−Cr(1)−O(1) 102.30(12), N(2)−Cr(1)−O(1) 96.58(12), N(3)−Cr(1)−N(1) 82.14(12), N(4)−Cr(1)−N(1) 82.78(13), N(2)−Cr(1)−N(1) 81.90(12).

Scheme 5

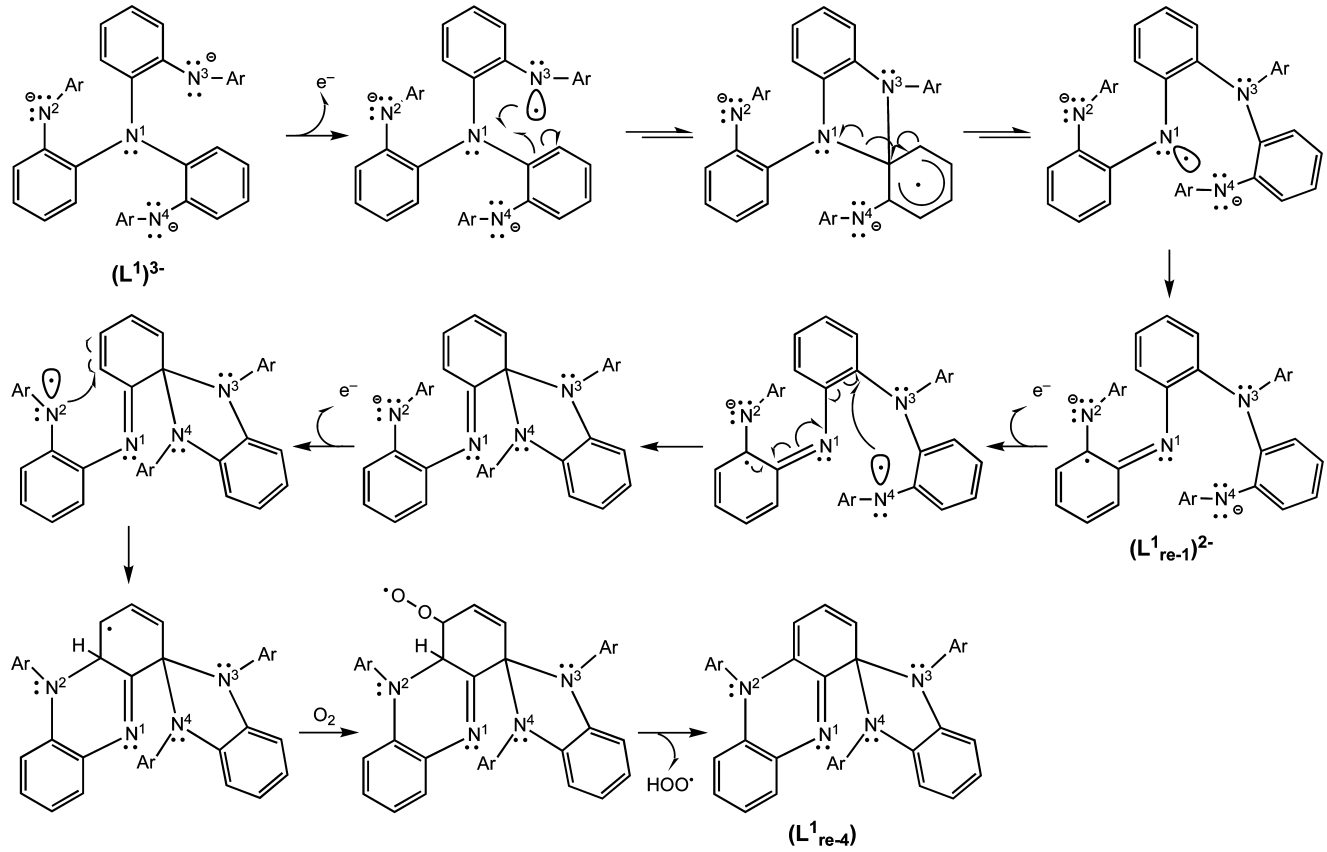

intricacies of assigning electronic structures to chromium complexes featuring ligand-centered radicals are nicely demonstrated in a recent publication by Wieghardt and co-workers.[33]

The structure of **4** (Figure 9) displays a distorted octahedral geometry, in which the axis defined by O(1)−Cr(1)−N(1) (175.31°) makes the closest approach to linearity. The ligand is rearranged as in compound **2** and also retains the one-electron oxidized *o*-disq$^-$ moiety between nitrogen atoms N(1) and N(2), as indicated by the average C−N distance of 1.361(6) Å and the pattern of four long (C(33)−C(34) 1.435(6), C(34)−C(35) 1.409(7), C(36)−C(37) 1.401(7), C(33)−C(38) 1.409(6) Å) and two short (C(35)−C(36) 1.356(7), C(37)−C(38) 1.378(7) Å) C−C bonds. On the other hand, the Cr(1)−N(1) and Cr(1)−N(2) bond distances (1.932(4), 1.959(4) Å) associated with the semi-imino residues are shorter than that observed for the genuine amido moiety (Cr(1)−N(4) = 2.019(4) Å). The shorter bonds can be explained by taking into account the position of atoms N(1) and N(2) trans to the weakly coordinating THF and $N(3)_{amine}$ moieties, respectively, whereas the location of atom N(4) is influenced by the strong trans effect of the coordinated chloride.

The structure of **5** (Figure 10) establishes that the ligand remains intact and that the compound possesses a distorted trigonal bipyramidal geometry with slight deviation from C_3 symmetry. The chromium ion lies 0.27 Å above the plane defined by the three sp^2 hybridized N_{amido} atoms in the direction of the coordinated THF. The average Cr−N_{amido} bond distance (1.957(3) Å) is similar to that encountered in **4**, but significantly longer than the corresponding average value of 1.877(3) Å reported for [Cr(III)(N_3N)] due to the reduced basicity of Ar_2N- moiety. Conversely, the weakened axial coordination of [Cr(III)(N_3N)] features a longer Cr−N_{amine} bond distance (2.243(3) Å) than that observed in **5** (2.094(3) Å).

Mechanistic Considerations. With reference to Scheme 5, the oxidative rearrangement of metallated ligand $[L^1]^{3-}$ to $[L^1_{re\text{-}1}]^{2-}$ has been previously established to occur via an initial one-electron transfer to an N_{amido} residue to generate an electrophilic aminyl radical. This *N*-centered radical then undergoes a 1,4-(*N*-to-*N*) phenyl migration, while the initial oxidation equivalent is retained in a newly formed disq$^-$ ring. Downstream oxidative events, leading to the metal-free $[L^1_{re\text{-}4}]$, most likely follow a similar pattern, enabled by initial oxidation of the genuine $N(4)_{amido}$ residue of **2**, which is electron-rich due to the weak coordination to Mn(III). The ensuing five-member imidazolato ring is trapped in $[L^1_{re\text{-}4}]$, since radical coupling is apparently preferred over ring opening. This process generates the central imino nitrogen N(1) of $[L^1_{re\text{-}4}]$, which then protects the adjacent carbon from repetition of the same process by the newly formed aminyl radical, generated by one-electron oxidation of the remaining

(30) Tsierkezos, N. G. *J. Solution Chem.* **2007**, *36*, 289–302.
(31) Schneider, S.; Filippou, A. C. *Inorg. Chem.* **2001**, *40*, 4674–4677.
(32) Filippou, A. C.; Schneider, S.; Ziemer, B. *Eur. J. Inorg. Chem.* **2002**, 2928–2935.
(33) Lu, C. C.; DeBeer George, S.; Weyhermüller, T.; Bill, E.; Bothe, E.; Wieghardt, K. *Angew. Chem., Int. Ed.* **2008**, *47*, 6384–6387.

amido residue. Instead, the aminyl radical adds to an ortho position to form the six-member ring. The removal of the bridgehead H atom is more contentious and is probably driven thermodynamicaaly by dioxygen addition to the allylic cyclohexenyl radical, followed by elimination of a hydroperoxyl radical. It is worthwhile noting that $[L^1_{re\text{-}4}]$ possesses structural elements of the celebrated Perkin's mauveine-type compounds.[34]

Conclusions

The following are the principal findings of the present study:

(1) Solutions of $[(L^1)Mn(II)\text{-}THF]^-$ (**1a**) in THF can be oxidized by dioxygen to afford the dioxo-bridged compound $[(L^1_{re-1})Mn(III)\text{-}(O)_2\text{-}Mn(III)(L^1_{re-1})][K(OEt_2)]_2$ (**2**). This compound contains a ligand that has been oxidatively rearranged, while retaining the oxidation equivalent as a π radical in a newly formed *o*-disq$^-$ moiety. The reduced basicity of the ligand and the steric encumbrance imposed contribute toward stabilizing the rare $Mn(III)(O)_2Mn(III)$ core.

(2) Compound **2** exhibits antiferromagnetic coupling, which is analyzed as being composed of a strong coupling between the $S = 1/2$ ligand-centered radical and the $S = 2$ Mn(III) ion and a more modest coupling between the two Mn(III) ions via the two oxo bridges. Compound **2** also shows rich electrochemical behavior, indicating storage of additional oxidation equivalents whose location is deemed to be ligand centered.

(3) $CrCl_3$ can provide the necessary oxidizing equivalent to oxidize compound $[(L^1)Cr(III)\text{-}THF]$ (**5**), featuring the intact C_3-symmetric ligand, to the corresponding six-coordinate species $[(L^1_{re-1})Cr(III)\text{-}(Cl)(THF)]$ (**4**). As with the case of manganese, one-electron oxidation above the Cr(III) level is ligand-centered, causing the same ligand rearrangement and retention of the oxidation equivalent as a π radical.

(4) The oxidation of the ligand is perceived to occur via an incipient metal-bound aminyl radical that is generated upon a one-electron ligand oxidation. This electrophilic radical is then engaged in rearrangement reaction, which amounts to an internal 1,4(*N*-to-*N*) radical aryl migration. The rearrangement gives rise to an *o*-diiminobenzosemiquinonate type moiety, which stabilizes the oxidation equivalent as a π radical.

Future studies will be directed toward elucidating the redox events above the $[[(L^1_{re-1})\text{-}M(III)]$ oxidation level, as suggested by current electrochemical results.

Acknowledgment. We thank Drs. Vassilis Tangoulis, Charles Barnes, Jeff R. Long, Louise Berben, Nicholas Leventis, George D. Chryssikos, Spyros Koinis, and Thomas Mavromoustakos for experimental assistance and useful discussions. We gratefully acknowledge generous financial support (to P.S.) by the NSF (CHE-0412959) and in part by the NIH/NIEHS (5 P42 ES007381). We also acknowledge NSF funding (CHE-0420497) for the purchase of the diffractometer at the University of Missouri-St. Louis.

Note Added after ASAP Publication. Due to a production error Chart 1, Schemes 3−5, and Figure 6 have been replaced in the version published ASAP October 21, 2008; the corrected version published ASAP October 28, 2008.

Supporting Information Available: X-band EPR spectra of **1a** in THF (Figure S1), IR spectrum of **2** (Figure S2), X-band EPR spectra of compounds **1a** and **2** after exposure to dioxygen (Figure S3), cyclic voltammogram of **3** (Figure S4), and X-ray crystallographic data for compounds **1**−**5** in CIF format. The material is available free of charge via the Internet at http://pubs.acs.org.

IC801219U

(34) (a) Seixas de Melo, J.; Takato, S.; Sousa, M.; Melo, M. J.; Parola, A. J. *Chem. Commun.* **2007**, 2624–2626. (b) Sousa, M. M.; Melo, M. J.; Parola, A. J.; Morris, P. J. T.; Rzepa, H. S.; Seixas de Melo, J. S. *Chem. Eur. J.* **2008**, *14*, 8507−8513.